# Histology-Compatible MALDI Mass Spectrometry Based Imaging of Neuronal Lipids for Subsequent Immunofluorescent Staining:

***Ibrahim Kaya[1], Wojciech Michno[1], Dimitri Brinet[1,2], Yasmine Iacone[1], Giulia Zanni[3], Kaj Blennow[1,4], Henrik Zetterberg[1,4,5], Jörg Hanrieder[1,4,5,6]***

[1] Department of Psychiatry and Neurochemistry, Sahlgrenska Academy at the University of Gothenburg, Mölndal, Sweden

[2] Department of Chemistry and Molecular Biology, University of Gothenburg, Sweden

[3] Karolinska Institute, Department of Women's and Children's Health, Karolinska University Hospital, Stockholm, Sweden

[4] Clinical Neurochemistry Laboratory, Sahlgrenska University Hospital, Mölndal, Sweden.

[5] Department of Molecular Neuroscience, Institute of Neurology, University College London, UK

[6] Department of Chemistry and Chemical Engineering, Chalmers University of Technology, Gothenburg, Sweden

**Corresponding Author**

Jörg Hanrieder, PhD

Department of Psychiatry and Neurochemistry, Sahlgrenska Academy at the University of Gothenburg, Mölndal Hospital, House V, Biskopsbogatan 27, SE-43180 Mölndal, Sweden

jh@gu.se; +46-31-343 2377

## ABSTRACT

Matrix assisted laser desorption/ionization imaging mass spectrometry (MALDI-IMS) enables acquisition of spatial distribution maps for molecular species in situ. This can provide comprehensive insights on the pathophysiology of different diseases. However, current sample preparation and MALDI-IMS acquisition methods have limitations in preserving molecular and histological tissue morphology, resulting in interfered correspondence of MALDI-IMS data with subsequently acquired immunofluorescent staining results. We here investigated the histology-compatibility of MALDI-IMS paradigm to image neuronal lipids in rodent brain tissue with subsequent immunohistochemistry and fluorescent staining of histological features. This was achieved by sublimation of a low ionization energy matrix compound, 1,5-diaminonapthalene (1,5-DAN), minimizing the number of low-energy laser shots. This yielded improved lipid spectral quality, speed of data acquisition and reduced matrix cluster formation along with preservation of specific histological information at cellular levels. The gentle, histology compatible MALDI IMS protocol also diminished thermal effects and mechanical stress created during nanosecond laser ablation processes that resulted in subsequent immuno fluorescence staining but not with classical H&E staining on the same tissue section. Furthermore, this methodology proved to be a powerful strategy for investigating β-amyloid (Aβ) plaque-associated neuronal lipids as exemplified by performing high-resolution MALDI-IMS with subsequent fluorescent amyloid staining in a transgenic mouse model of Alzheimer's disease (tgSwe).



**Keywords:** MALDI imaging mass spectrometry (IMS), immunohistochemistry, histology, tissue integrity, laser ablation on biological tissues, Alzheimer's disease (AD), amyloid beta (Aβ) plaques, Amyloid-β Plaque Associated Neuronal Lipids

# INTRODUCTION

Lipids are the most abundant components of neural cell membranes, having a variety of functions in neurobiological processes including metabolism, cell adhesion and migration, signal transduction, and apoptosis.[1-3] Moreover, they may play roles in the pathogenesis of many neurodegenerative diseases, such as in Alzheimer's disease[4], Parkinson's disease[5], amyotrophic lateral sclerosis (ALS)[6] and multiple sclerosis (MS)[7], which all show lipid alterations in the central nervous system.[4, 5, 8] Therefore, to investigate the spatial distribution of neuronal lipids and to disentangle their functional roles *in situ*, advanced chemical imaging techniques, such as imaging mass spectrometry (IMS), are required.[9, 10]

IMS allows for examining the molecular architecture in complex biological matrices and hence often referred to as molecular histology.[11] The technique can be used for spatial mapping of neuronal molecules in mammalian brain tissue[10, 12, 13], which can be employed in the study of neurodegenerative diseases.[14, 15] MALDI-IMS has been several times demonstrated to be an effective tool for probing of neuronal lipids[11, 14], peptides[16, 17] and proteins *in-situ*.[9, 18] For MALDI-IMS, a desorption enhancing photon-absorbing matrix compound[19] is applied onto tissue section

Many sample preparation methods have been developed for improving MALDI-IMS performance in order to enhance the analyte signal-to-noise (S/N) ratio, minimize analyte delocalization and provide high spatial resolution for lipid molecular species in different tissue types.[20, 21] In these studies, homogeneous matrix coating has been addressed as a crucial step in terms of high spatial resolution. It has been concluded that most matrix coating methods including use of solvents have a risk of analyte delocalization, in particular for small molecules (e.g. lipids). Therefore, dry matrix coating strategies have been developed for high-spatial resolution analysis. Sublimation is a solvent-free, dry approach for matrix application in MALDI-IMS[21] and was demonstrated to give the best data in terms of signal

quality and ion image resolution for lipid molecules allowing improved correlation with histological information.[20, 22]

In most MALDI imaging studies, histological staining with e.g. hematoxylin and eosin (H&E) is commonly performed following the MALDI-IMS analysis on the same tissue section in order to correlate ion image data with histological features.[23, 24] While H&E staining is a histological staining technique to evaluate cell and tissue structures, it is not specific to distinct protein epitopes as immunohistochemistry (IHC). However, IHC and fluorescent staining following MALDI-IMS analysis on the same tissue sections can be challenging due to the potential tissue distortion and epitope degradation as a consequence of laser ablation.[25] Here, mechanical stress along with thermal denaturation effects induced by nanosecond pulse laser ablation[25, 26] is likely to impact the morphology, integrity and molecular composition of histological tissue section. Consequently, this can impair accurate correlation between MALDI-IMS and histological staining data. As a result, the laser ablation process on biological tissues should be taken into consideration for efficient multimodal imaging analysis schemes, as this can be a major reason for inconclusive correlations. Currently, there are only few reports on subsequent immunofluorescent staining following MALDI-IMS analysis on the same tissue section, with in part inconclusive IMS/IHC correlation results.[14, 17, 27] We previously studied amyloid-plaque associated neuronal lipids and amyloid-β peptide species in transgenic Alzheimer's disease (AD) mice using MALDI-IMS of lipids[14] and peptides[17] followed by immunofluorescent staining of plaques on the same section. Although co-localization of MALDI ion images and fluorescent amyloid images was obtained in these studies for qualitative validation, the IMS/IHC signal alignment was not optimal at higher resolution scales. [14, 17] This was particularly prominent for peptide imaging as these MALDI experiments require higher laser pulse energies for desorption-ionization of large peptides and proteins.[28] Since, all of these studies employed a nanosecond Nd:YAG laser with structured beam profile, [29] it is relevant to consider the local mechanical and

thermal denaturation effects during laser ablation process to enhance MALDI-IMS compatibility for subsequent immunofluorescent staining.

The aim of the present study, was to therefore to investigate the histology compatibility of sublimation based matrix deposition for MALDI-IMS spatial profiling of neuronal lipids with subsequent multiplexed immunofluorescent staining in mice brain. Here, sublimation with 1,5-diaminonapthalene (1,5-DAN) as MALDI matrix was found to give the best lipid signals in both ionization modes using low laser pulse energies and number of laser shots. This further resulted in minimal damage in tissue integrity and morphology for follow up immunofluorescent staining on the same tissue. In addition, the final method was exemplified on a transgenic Alzheimer's disease mice model (tgSwe) to examine cortical Aβ plaque pathology-associated lipid profiles *in situ.*

## EXPERIMENTAL SECTION

**Chemicals and Reagents.** All chemicals for matrix and solvent preparation were pro-analysis grade and obtained from Sigma-Aldrich (St. Louis, MO), unless otherwise specified. TissueTek optimal cutting temperature (OCT) compound was purchased from Sakura Finetek (AJ Alphen aan den Rijn, The Netherlands). The *dd*H2O was obtained from a MilliQ purification system (Merck Millipore, Darmstadt, Germany).

**Animals.** C57BL/6 female mice from Charles Rivers Laboratories were used for method development (Sulzfeld, Germany). The animals were housed at the animal facility in Gothenburg (Laboratory of Experimental Biomedicine, EBM), kept under standard conditions of daylight (12-hour light cycle) and provided with food and water *ad libitum*. Animals were delivered with their respective dams that were further separated at postnatal day (PND) 21 of the pups. For the analysis, animals were anesthetized with isoflurane and killed by decapitation.

Transgenic AD mice, 18 months of age, carrying the Swedish mutation (K670N, M671L) of human APP (tgSwe) were used and reared ad libitum at the animal facility at Uppsala University under a 12/12-hlight/dark cycle.[30] All experimental conditions were approved by the Animal Research Ethics Committee (Gothenburg committee of the Swedish Agricultural Agency and Uppsala University), in accordance with the national animal welfare legislation. The following ethical identification number was used: (DNr #20-2013, Gothenburg; DNr #C17⁄14, Uppsala University).

**Tissue Sampling and Sectioning.** The brains were dissected quickly with 3 minutes postmortem delay and frozen on dry ice. Frozen tissue sections (12µm) were cut in a cryostat microtome (Leica CM 1520, Leica Biosystems, Nussloch, Germany) at 18°C, and collected on special-coated, conductive ITO (indium tin oxide) coated glass slides (Bruker Daltonics, Bremen, Germany) and stored at -80°C. Prior to matrix deposition by sublimation, tissue sections were thawed in a desiccator for 30 minutes under reduced pressure (SpeedVac, Eppendorf, Hamburg, Germany).

**Sublimation based Matrix Deposition.** Matrix deposition was carried out in a sublimation apparatus (Sigma Aldrich) as previously described.[14] The sublimation protocol was optimized with respect to temperature, deposition time and total amount of deposited matrix in order to obtain the best detection efficiency for lipids on mice brain tissue. Under stable vacuum (0.8 mbar) and temperature (130°C) conditions, we varied the amount of matrix coating between 50 and 300µg/cm$^2$. A too thin matrix layer (50-70µg/cm$^2$) yielded very few lipid ions, while a too thick matrix layer (200-300µg/cm$^2$) resulted in dominant matrix ions (Supporting Information, Figure S-1). With this setup, the optimum matrix layer was found to be 120µg/cm$^2$ to give the best lipid signals, which is in a good agreement with previous results[31]. We used optimized sublimation conditions: 20 minutes at a temperature of 130°C under a stable vacuum of 0.8 mbar. Homogeneity of the matrix distribution over the analyzed

sections was evaluated by monitoring the non-normalized ion intensity of a proposed matrix derived $[2DAN-2H]^{+\cdot}$ Ion. [31] (Supporting Information Figure S-2).

**MALDI-IMS Analyses.** Imaging MS analysis of tissue sections were performed on a MALDI TOF/TOF UltrafleXtreme mass spectrometer equipped with SmartBeam II Nd:YAG/355 nm laser operating at 1 kHz providing a laser spot diameter down to ~10µm for the 'minimum' focus setting (Bruker Daltonics).[29] As the laser beam energy profile (structured) and instrumental setup of the here used MALDI instrumentation do not facilitate straight forward measurement of exact laser fluence value at a flat target surface, [29] detailed information about the laser pulse energy settings is provided as follows: Global laser attenuator setting was kept stable at 10% throughout all the experiments and the laser focus set to minimum. Attenuator offset was 40% and attenuator range was 10%, for the minimum laser focus. The laser shot count of the instrument unit used for this experimentation was about 1501245k (in ~9 months age).

The effect of laser energy and number of shots on matrix cluster intensity was evaluated on blank glass slides covered with 120µg/cm$^2$ sublimated matrix. Varying laser pulse energies (5% increments over attenuator range: 0 to 100%) with n=10 shots were investigated and number of laser shots (5, 20, 50, 100, 300, 500) were evaluated at threshold laser energy (global offset 10% and attenuator offset 40% with the attenuator/density wheel set to 0%). Here the signal intensity (SI) of all 1,5-DAN matrix derived cluster peaks was determined using peak picking (centroid, S/N 3) in flexAnalysis (v 3.0, Bruker Daltonics). The mean values were statistically compared using ANOVA and Tukey posthoc analysis in origin (v8.1 originlab, Northampton, MA).

MS data acquisitions were performed in reflective ion mode over a mass range of 300-2000 Da with a source accelerating voltage of 25kV in positive and 20kV in negative polarities. The detector gain value was kept stable at 2626 V for both ionization modes. A mass resolution of M/ΔM 20 000 was achieved in the lipid mass range (i.e., 650−1000 Da). External

calibration was carried out using peptide calibration standard I (Bruker Daltonics). Image data were reconstructed, root mean square (RMS) normalized and visualized using Flex Imaging v3.0 (Bruker Daltonics). Lipid classifications were determined by comparing mass accuracy data with the LIPID MAPS database (Nature Lipidomics Gateway, www.lipidmaps.org).

**Immunohistochemistry/Fluorescence and H&E Staining.** Prior to staining, sections were rinsed in absolute EtOH for 60s, fixed in 95%EtOH/5%AcOH at -20°C for 9 min, 70%EtOH at -20°C for 30sec, 70%EtOH at RT for 30sec, followed by 5min PBS, and 5min PBST (0.1% v/v Tween 20) wash at RT. Tissue was blocked for 1 hour at RT with blocking solution (PBST, 5% NGS, 2% BSA), followed by overnight primary antibody incubation at 4°C. The following morning, sections were washed 3x5min with PBST and stained with fluorescent secondary antibodies for 1h at RT. Finally, tissues were washed 3x5min with PBST, and mounted with Prolong Gold Antifade Mountant with 4',6-diamidino-2-phenylindole (DAPI, Thermo Fisher Scientific, Waltham, MA). Both primary and secondary antibodies were diluted in PBST containing 0.05% NGS, 0.02% BSA. Anti-βIII-tubulin (1:250, Abcam, Cambridge, UK) and Anti-Glial Fibrillary Acidic Protein (GFAP, 1:500, Abcam,) primary antibodies were used. Goat anti-rabbit IgG conjugated to Alexa Fluor 488 (Thermo Fisher Scientific) and goat anti-mouse IgG conjugated to Alexa Fluor 555 (Thermo Fisher Scientific) were used for visualization. Sections stained in diluent solution without primary antibodies, served as negative control. Imaging was performed using a wide field microscope (Axio Observer Z1, Zeiss, Jena, Germany) using 10x air objective for overview images and 100x oil objective for investigation of laser ablation effects. Image processing was done using the ImageJ software (http://rsb.info.nih.gov/ij/). For H&E staining, after MSI the matrix was washed away using 2x1 minute submersions in 100% EtOH. Tissue was rehydrated in 70% EtOH, 50% EtOH and milliQ water, 2 minutes each. The slide was placed in hematoxylin (HistoLab Products, Västra Frölunda, Sweden) for 2 minutes and washed with water for 2 minutes. The slide was then counterstained in 0.2% Eosin (HistoLab Products) for 2 minutes and washed in water for 2 minutes. The section was finally washed and dehydrated in

50%EtOH, 70% EtOH and 100% EtOH for 1 minute each. Tissue was mounted with Permount mounting medium (eBioscience, Thermo Fisher Scientific). For fluorescent amyloid staining, after MALDI-IMS analysis, sections were rinsed in absolute EtOH for 60s, fixed in absolute EtOH at −20 °C for 8 min, 70%EtOH at −20 °C for 30 s, 70%EtOH at RT for 30 s, and rinsed for 5min in PBS both prior and after staining. For amyloid staining, 30 min incubation in heptameric formyl-thiophene acetic acid (h-FTAA), diluted to a final concentration of 3 mM in PBS, was used. Prior to imaging, the tissue was mounted with Prolong Gold antifade reagent (Thermo Fisher Scientific) and dried for 2 h at RT. Imaging was performed using a wide field microscope (Zeiss Axio Observer Z1).

## RESULTS AND DISCUSSION

In the present study, we investigated the suitability of high spatial resolution lipid imaging using MALDI IMS for subsequent immunofluorescent staining. To overcome lateral analyte diffusion issues as commonly observed with wet matrix coating approaches (e.g. nebulizers and airbrushes), we investigated sublimation based approach for matrix deposition and lipid imaging prior to subsequent immunohistochemistry and fluorescent staining. Histology-compatibility of laser ablation process has been studied in detail.

### Reducing Matrix Cluster Formation Induced by Laser Irradiation.

Interaction of laser energy with matrix compounds is the crucial step for enhanced ion yields in MALDI-MS analysis since all matrix compounds have different optical and physico chemical properties.[32] In the present study, commonly used matrix compounds, including DHB, HCCA and 1,5-DAN were investigated for sublimation and neuronal lipid imaging in rodent brain in both ionization modes. The sublimation protocol was used with optimized amounts of deposited matrix in accordance with previously described results.[31] Here, sublimation of DHB and HCCA gave poorer lipid spectral quality (600-1000Da) with the

same laser fluences as compared to 1,5-DAN sublimation and MALDI IMS, particularly in negative ion mode (Supporting Information Figure S-3). In UV-MALDI, increased laser fluences result in high-intensity matrix signals beside fragmentation of matrix- and analyte molecules, which causes deterioration of the spectral quality and matrix suppression effect.[32, 33] Indeed, even slightly increased laser fluences resulted in matrix cluster formation when using sublimation of 1,5-DAN for MALDI IMS (Figure 1).

Upon laser irradiation, 1,5-DAN shows a unique behavior with respect to radical formation in contrast to other matrix compounds. Odd-electron radical ion species are $M\text{-}H^{+\cdot}$ readily formed rather than $M\text{-}H^{+}$ ions, which is justified by its low ionization energy.[31] We investigated the effect of laser pulse energy and number of laser shots on the total signal intensity of matrix derived signals from sublimation based matrix deposition. Increasing laser pulse energy and number of laser shots resulted in a sharp increase in the total signal intensity of all matrix derived signals in both positive and negative polarities (Figure 1).

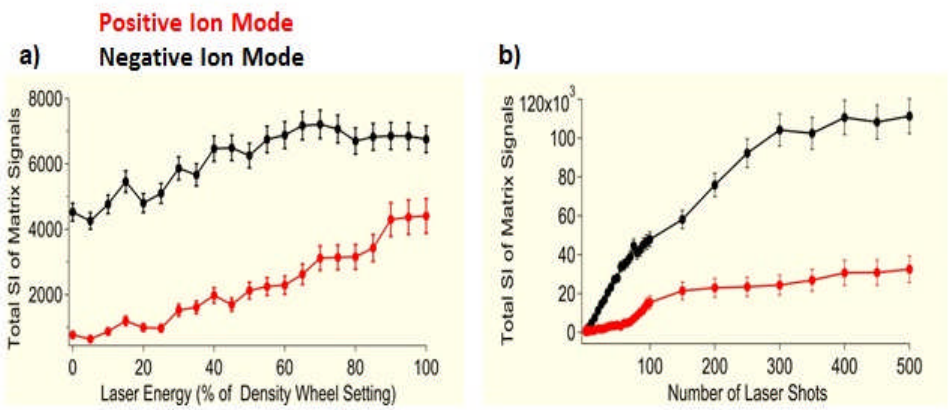


**Figure 1.** Effect of a) laser pulse energy (10 laser shots) and b) number of laser shots (at threshold laser pulse energy) on the total signal ion intensity of matrix derived peaks from a sublimation based matrix coating (120µg/cm$^2$). Data collected both in positive (red) and negative (black) ionization modes. Error bars: SD, (n=3). For both ion modes, statistical significance ($p<0.05$) was observed e.g. between 0 and 15% and 0 and 30% in a) as well as for 0 and 100 shots in b).

Formation of matrix cluster ions was more prominent in negative ionization mode at the same levels of laser fluences as compared with positive ionization mode (Figure1). This could be explained by distinct reductive properties and radical ion transfer abilities of 1,5-DAN compared with other matrices.[31, 34] Here, negative radical species produced by laser irradiation ($M^{\cdot -}$) were shown to cause further reduction reactions via producing $H^{\cdot}$ radicals.[31] This can in turn give rise to a larger number and more intense peaks of negatively charged matrix cluster ions as compared with positively charged cluster ion species. Therefore, using 1,5-DAN as a MALDI matrix could facilitate efficient gas phase ionization of lipid species with readily ionized 1,5-DAN matrix ions with very low-energy laser irradiation, particularly in negative ionization mode.

**Histology Compatibility and Spectral Quality of MALDI-IMS.** Beyond extensive matrix cluster ion formation and diminished sensitivity by oversampling[35], high laser pulse energies and large number of laser shots have a severe impact on tissue integrity and morphology. This in turn may result in poor histological information after MALDI-IMS analysis. Again, the choice of matrix is very relevant as it can have a substantial effect with respect to tissue distortion during desorption-ionization process due to the distinct molar UV absorptivity values and other physicochemical properties of the different UV absorbing matrix compounds.[32] For the here investigated matrices, DHB, HCCA and 1,5-DAN, DHB and HCCA gave inferior lipid signal intensities (Supporting Information Figure S-3), which in turn would require higher laser energies for DHB and HCCA in order to obtain a comparable IMS spectral quality. This further supports the hypothesis that 1,5-DAN based MALDI is characterized by more gentle desorption and ionization process as compared to other matrices. Moreover, the reduced laser energy and number of shots used for 1,5-DAN might result in reduced tissue distortion as compared to DHB and HCCA, where higher laser energies are needed.

In order, to investigate the histology-compatibility of MALDI-IMS analysis, four different regions within a mouse brain cerebellum, including the molecular and granular layers of the cerebral cortex and the cerebral white matter (Figure 2a). The regions were analyzed with different MALDI parameters in negative polarity using 1,5-DAN sublimation. This included varying laser pulse energies and number of laser shots (Figure2b,c). The impact on tissue morphology was then evaluated by means of subsequent IHC and fluorescent staining experiments (Figure 2a).

Here, we observed that high laser pulse energies (50% density wheel) resulted in tissue distortion with 5 and 100 laser shots (Figure 2a I-II). Moreover, this was accompanied with poor MALDI-IMS image quality (Figure 2b I-II) as well as higher number and intensity of 1,5-DAN cluster ions in between 300-650 Da mass range (Figure 2c I,II). These extensive clusters resulted furthermore in suppressed lipid signals (Figure 2c I,II). In contrast, MALDI experiments with low laser pulse energy (threshold energy level), were efficient to protect tissue integrity (Figure 2a III-IV) and improved MALDI imaging data. However, a higher number of low-energy laser shots (100) still resulted in image distortion, showing signs of laser ablation in the IHC images (Figure 2a III) and intense matrix clusters between 300-650 Da (Figure 2c III).

On the other hand, cerebral white matter was found to be more resistant to higher laser pulse energies and higher number of laser shots, showing less signs of damage compared to molecular and granular layers (Figure 2a I-II). This fact points out the great importance of mechanical properties of biological tissues to laser ablation, as both the elasticity and strength of the tissues can modulate the kinetics and dynamics of the ablation process.[25] The resistant of white matter to the energetic laser pulses and local heating by nanosecond pulse durations can be explained by the superior rigidness as this region consists mainly of myelinated fiber tracts.[36] In turn, the higher susceptibility to laser ablation effects for the

molecular- and granular layer can be explained by their soft tissue properties as these layers consist mainly of cell bodies [25] with less myelin content.[36]

Laser ablation effects on tissue morphology were further investigated on different areas of molecular layer within the cerebellum in a sagittal mouse brain tissue section. By varying the number of laser shots (5, 20, 50, 100, 200, 300, 500) using threshold laser energy, tissue and fluorescent signal distortions were observed starting with 50 laser shots and getting prominent with ≥100 laser shots (Supporting Information Figure S-4I-II). Moreover, epitope degradation was prominent as indicated by the decreased tubulin and GFAP immunofluorescence, while the DAPI signal was less affected (Supporting Information Figure S-4II). In addition, control experiments were performed to investigate whether the increased fluorescence background on the laser ablation sites is a result of sole tissue damage and autofluorecence or non-specific binding of primary and secondary antibodies on the ablated raster sites. Therefore, control experiments were performed without using any or solely a secondary antibody following MALDI-IMS analysis with varying number of laser shots. The results indicate that ablation-damaged tissue areas display increased background in both blue and green channels in fluorescence microscope images (Supporting Information Figure S-5II), while no significantly higher fluorescent signal was observed with staining using the fluorescently labelled secondary antibody (Supporting Information Figure S-5I). This suggests a dominant effect of tissue distortion and consequently autofluorescence rather than unspecific binding (Supporting Information Figure S-5).

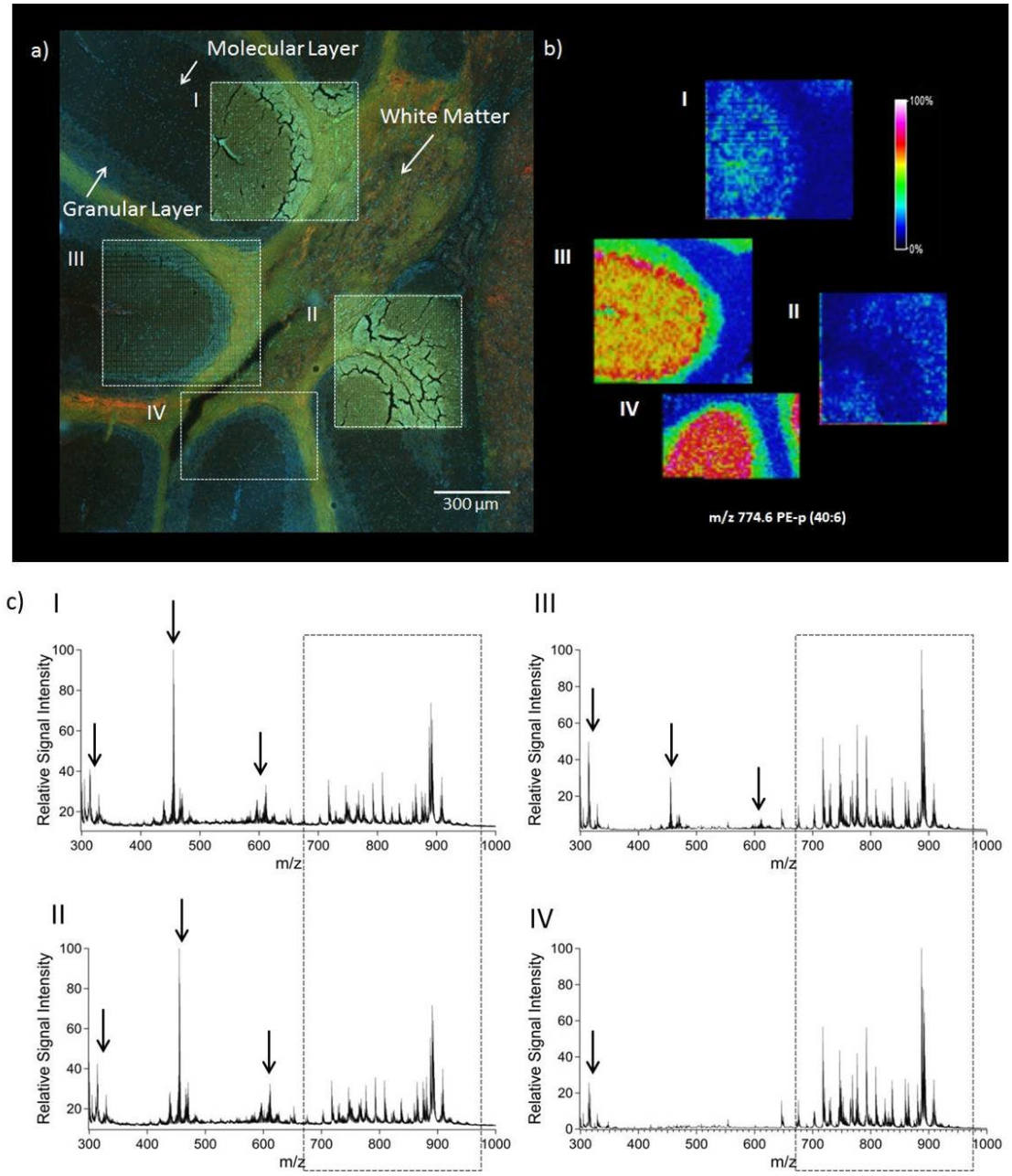


**Figure 2.** Subsequent IHC and fluorescent staining images of four different sections on mice cerebellum region analyzed with different parameters of MALDI imaging mass spectrometry. a I) 100 of 50%-energy laser shots a II) 5 of 50%-energy laser shots a III) 100 of threshold-energy laser shots and a IV) 5 of threshold-energy laser shots in reflective negative ion mode followed by immunohistochemistry and fluorescent staining. Corresponding single ion images of PE-p (40:6, m/z 774.6) and full range MS spectra of the same sections were shown in b I-IV and c I-IV, respectively. Highlighted regions in the spectra (650-950 Da) show relative signal intensity of lipids. Arrows in between 300-650 Da mass range indicate 1,5-DAN matrix cluster ions. %-energy stands for density wheel setting. Imaging data were acquired with a spatial resolution of 10µm. Anti-glial fibrillary acidic protein (GFAP, green), anti-βIII-tubulin (red) and fluorescent stain 4,6-diamidino-2-phenylindole (DAPI, blue) were used to visualize radial glial cells, cytoskeleton and cell nuclei, respectively; allowing to highlight the molecular layer, the granular layer and the white matter.

Interestingly, using solely threshold laser energy (i.e. global offset: 10%, attenuator offset: 40%, 0% density wheel), with only 5 laser shots, proved to maintain histological morphology

with an undistorted image quality and fluorophore signal as well as protection of protein epitopes (Figure 2a IV). These parameters resulted in enhanced spectral information and IMS data quality (Figure 2b IV), which is further highlighted by the single ion images of phosphatidylethanolamine (PE-p 36:4) indicating a substantial signal increase of this species in the molecular layer (Figure 2b IV). Moreover, this approach resulted in a general enhancement of lipid signals (in 650-950 Da mass range), as compared to collection of 100 laser shots, along with suppression of matrix clusters between 350-650 Da (Figure 2c IV).

These results can be explained by the comparable low ionization energy of 1,5-DAN. Although understanding of desorption/ionization process is still unachieved due to the complex ionization processes in desorbed matrix-assisted laser desorption plume[28, 37], analyte ion formation in UV-MALDI was shown to be a convolution of analytes pre-charged in the solution (Lucky-Survivor Model) [38] as well as ionization of neutral analytes by the ionized matrix ions in the gas phase. [37, 39, 40] Therefore, low energies sufficient for ionization of 1,5-DAN molecules can enhance gas phase ionization of lipids by readily ionized matrix ions even at very low laser fluences, particular in negative ion mode. As a result, by minimizing the oversampling effect and to increase the ionization sensitivity [35], this “gentle” irradiation does further enable improved correlation of well-preserved molecular tissue morphology with lipid signals, as illustrated for PE-p (40:6, m/z 774.6) species.

**Microscale Effects of Laser Ablation following MALDI-IMS.** Using only a low number of laser shots at low laser pulse energies allowed for comprehensive MALDI-IMS and subsequent fluorescence microscopy of the molecular layer, granular layer and the white matter of the cerebellum, as visualized with antibodies towards glial fibrillary acidic protein (GFAP) and βIII-tubulin as well as DAPI for nuclear staining (Figure 3).

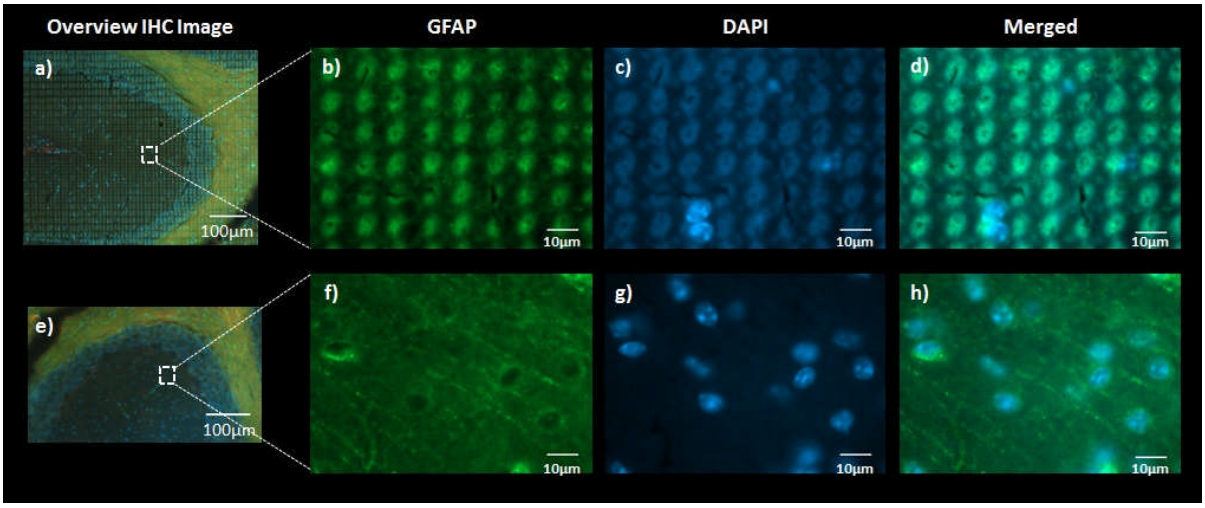


**Figure 3**. High resolution immunohistochemistry and fluorescent staining images following MALDI-IMS. Immunohistochemistry and fluorescent staining were performed on two cerebellar regions of interest (ROI-I: a-d, corresponding to Fig. 2a-III and ROI-II: e-h, corresponding to Fig. 2a-IV). High resolution fluorescent microscopy (100x) shows no overlap of laser ablation after MALDI-IMS with (b-d) 100 shots and (f-h) 5 shots with laser energy set to threshold (0% density wheel setting). (f-h) Low number of laser shots at threshold energy allowed for visualization of radial glial cells (GFAP, green) and cell nuclei (DAPI, blue) without laser ablation damage on the brain tissue as compared to b-d where tissue distortion is observed. Magnification a,e: (10x); b-d, f-h: (100x).

In particular, by using a higher magnification (100x), a clear visualization of cellular structures including nuclei (DAPI) and cytoplasmic protein accumulation (GFAP) was possible as laser ablation induced interferences on the tissue surface were abolished, when acquiring IMS data with only 5 laser shots (Figure 3 f-h) as compared to collection of 100 shots (Figure 3 b-d). The results highlight that the application of 1,5-DAN sublimation and gentle laser irradiation for lipid MALDI-IMS in negative ion mode preserves the entire histological information for subsequent IHC analysis and suggests thereby enhanced correlation of molecular information with histological features.

On the other hand, the IHC results were compared to H&E staining following MALDI IMS. H&E is commonly used after MALDI-IMS analysis on the same tissue section to correlate IMS data with histological features.[23] It is a non-specific chemical staining method, which is used to evaluate all histological structures and cells that take up the staining dye. As this is a general protein staining method, i.e. not specific for any unique epitope(s), it may not reveal distortions of protein structures and cells occurring as a consequence of laser ablation

effects caused by irradiation with energetic laser pulses during desorption-ionization process.

Indeed, in contrast to IHC and fluorescent staining, high resolution microscopy images of subsequent H&E staining did not show any laser ablation effects on tissue morphology when acquiring MALDI-IMS data with 200 laser shots per pixel area at threshold laser pulse energy (Figure 4). Furthermore, control experiments have been performed using exactly the same tissue pre-treatment for both H&E and IHC staining experiments. Laser ablation effects on the tissue morphology were further investigated on different sections of molecular layer with varying number of laser shots (5, 50, 100, 200, 300, 500) using threshold laser energy. Here, high-resolution microscopy images of H&E staining indicated no signs of laser ablation effects up to 500 laser shots (Supporting Information Figure S-6).

These results can be explained by the non-specific staining of H&E in which hematoxylin and eosin stain general nucleic acids and proteins [41]. H&E staining involves application of hemalum that stains nuclei of cells (and a few other objects, such as keratohyalin granules and calcified material).The nuclear staining is followed by counterstaining with an aqueous or alcoholic solution of eosin Y, which stains eosinophilic structures in various shades of red, pink and orange.[41] Interestingly, in the fluorescent staining experiments, the DAPI staining intensity was largely unaffected as compared to the antibody labelling (Figure 3c and Supporting Figure S4). This further supports the theory that epitope availability is more sensitive to laser ablation effects than unspecific histological staining as observed for DAPI and H&E.

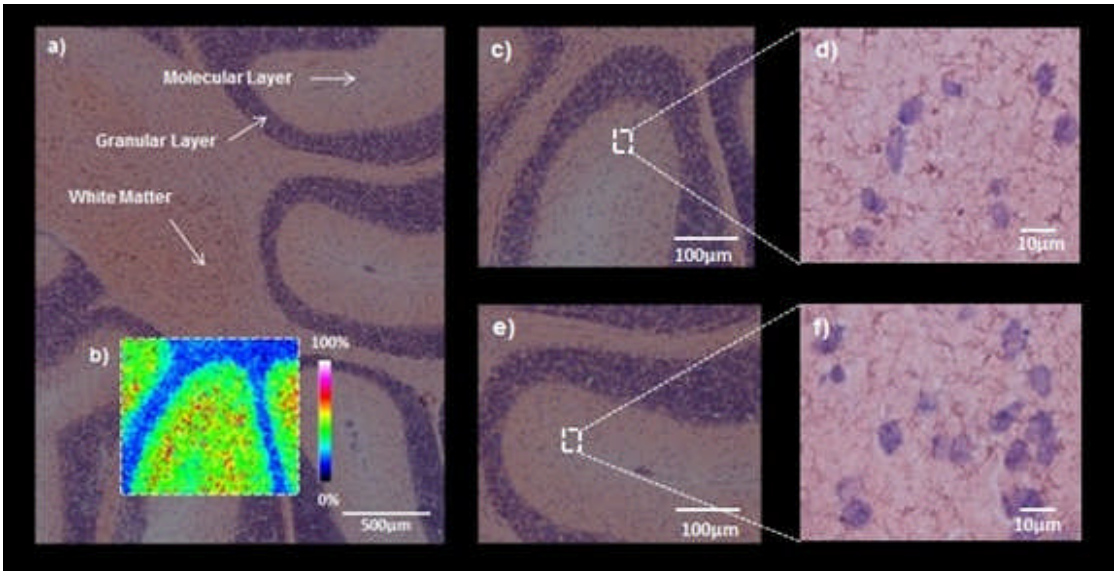


**Figure 4.** High resolution H&E staining after MALDI-IMS analysis on the same tissue section. a) H&E stained cerebellar region. b) Single ion image of PE-p 40:6 (m/z 774.6) from cerebellar region analyzed with MALDI-IMS by acquiring 200 laser shots (at threshold laser pulse energy) per pixel with 10µm spatial resolution. High resolution microscopy images of (c,d ) MALDI-IMS analyzed and e, f) non-analyzed regional microscopy images show no laser ablation effects with c,e) 20x and d,f) 100x magnification.

This in turn is of great relevance, as MALDI imaging applications are commonly based on subsequent H&E staining in order to validate and correlate the ion signals to histopathologically relevant features. As H&E staining is unspecific, consequences of tissue distortion and ion delocalization cannot be detected and quantified. This can in turn lead to misalignment issues and false positive results for correlation of multimodal imaging data and biological interpretation (Figure 4c,d).

**High Resolution MALDI IMS with Subsequent Immunofluorescent Staining.** High-resolution MALDI-IMS is a suitable approach for improved correlation of MS ion image data with histological features.[11, 42] We achieved a spatial resolution of 10µm in both positive and negative ionization modes to reach spatially detailed information to be correlated with histological features which were visualized by subsequent IHC and fluorescent staining (Figure 5a, b). In this case, when using minimum laser focus parameter, no laser ablation overlap was observed with 100 of low-energy laser shots (Figure 3a-d) and even no signs of

laser ablation with low-energy few number of laser shots (Figure 3e-h) in negative ionization mode. Using 1,5-DAN sublimation in conjunction with gentle irradiation in MALDI-IMS analysis of neuronal lipids allowed for subsequent immunohistochemistry analysis with minimized loss of histological information in negative ion mode (Figure 5a). However, the number of laser shots (n=50) at the threshold laser energy (global offset: 10%, att. offset 40%, 0% density wheel) that was needed to obtain intense lipid signals was higher in positive ion mode. This can be due to the fact that 1,5-DAN as a basic matrix compound can act as a ‘‘proton sponge’’ during desorption-ionization process and suppress the formation of positively charged lipid ions in the gas phase. Therefore, in positive ion mode, slight signs of laser ablation effects were observed on the tissue surface after high resolution MALDI-IMS analysis. (Figure 5b)

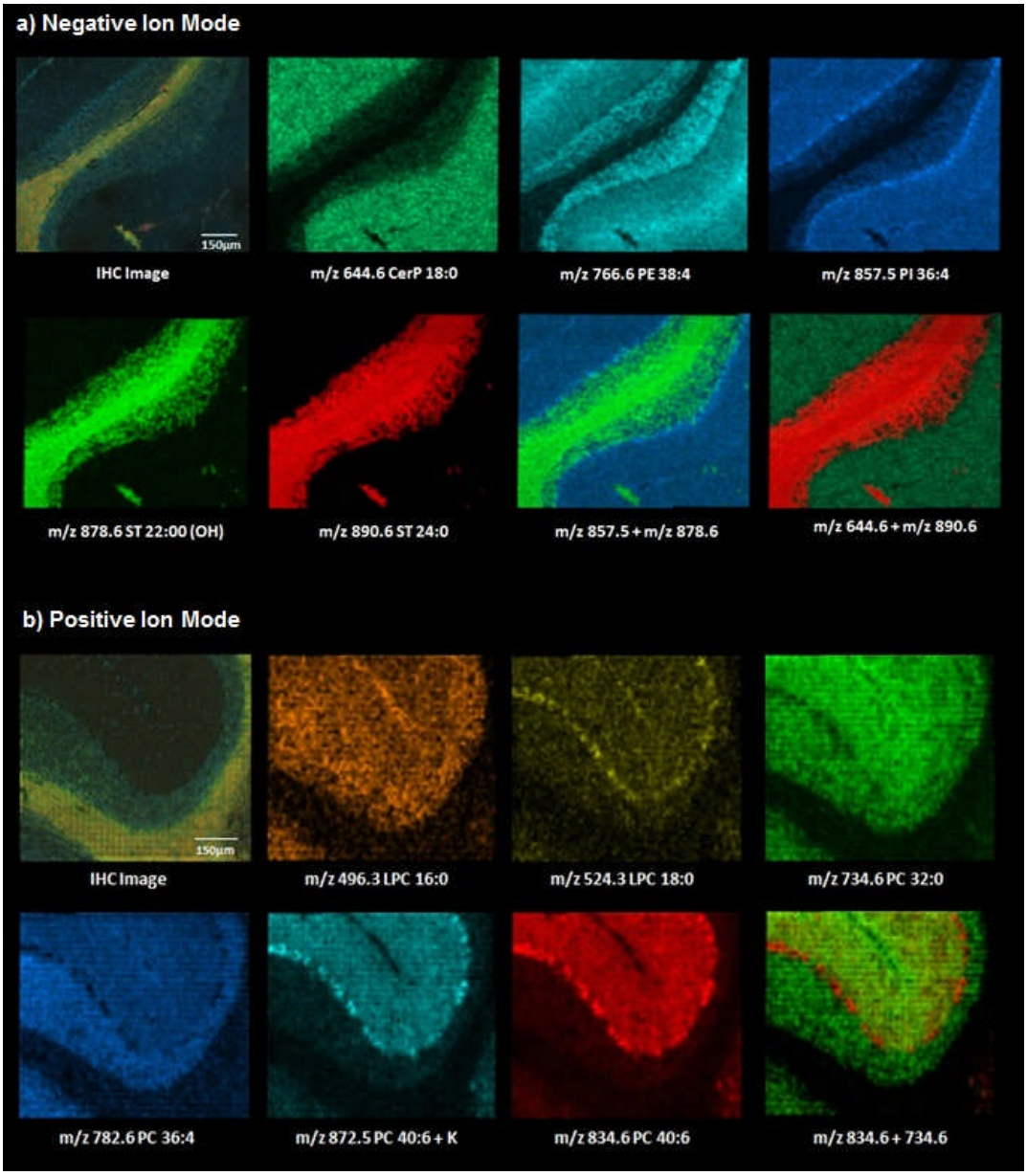


**Figure 5.** High spatial resolution MALDI-IMS of lipids in both a) negative and b) positive ionization modes from a sagittal mice cerebellum regions coated with 1,5-DAN sublimation approach and acquired with a lateral resolution of 10µm. Anti-glial fibrillary acidic protein (GFAP, green), anti-βIII-tubulin (red) and 4,6-diamidino-2-phenylindole (DAPI, blue) fluorescent stain were used to visualize radial glial cells, cytoskeleton and cell nuclei, respectively; allowing to highlight the molecular layer, the granular layer and the white matter.

Here histological features of the of the cerebellar regions as outlined by fluorescence immunostaining can be visualized and correlated with ion signals of distinct neuronal lipid species, including ceramides (CerP 18:0, m/z 644.6), sulfatides (ST 20:4, m/z 890.6) and phosphoethanolamines (PE 38:4, m/z 766.6) and phosphoinositols (PI 36:4, m/z 857.5) in negative ion mode (Figure 5a) and phosphatidylcholines (PC 32:0, m/z 734.6) and

lysophosphatidycholines (LPC 16:0, m/z 496.3 and LPC 18:0, m/z 524.3) in positive ion mode (Figure 5b). In detail, PE 38:4 and PC 36:4 were found to localize to the cell body dense granular layer as visualized with DAPI, highlighting their role in mammalian neuronal cell membranes. In addition, together with CerP 18:0 and PC 40:6, these species also localized to the radial glial cell rich molecular layer, as visualized with GFAP, also known for presence of granule cell derived parallel fibers. In contrast, sulfatides ST 24:0 and ST 22:0(OH) predominantly localized to the white matter and in part to the granular layer. This can be tied to the abundance of long myelinated axons in the white matter (as visualized with anti-βIII-tubulin) and presence of oligodendrocytes in the granular layer where sulfatides are one of the main lipid constituents.[43]

**Enhanced Speed of Data Acquisition for High Spatial Resolution in Negative Ionization Mode.** High-speed in IMS is needed in order to obtain high spatial resolution ion images of larger tissue areas in a reasonable acquisition time[35], particularly for sublimated tissue samples, where volatile matrices are used that are subjected to high vacuum in the ion source.[44] For example, acquisition of a small cerebellar region requires 8412 pixel points to be analyzed with 10μm spatial resolution (Figure 6a). For high-speed MALDI-TOF IMS, there have been technological advances including high repetition rate lasers, continuous raster sampling, and synchronized high repetition laser beam with rapidly moving sample stage.[35, 44, 45] However, the number of laser pulses required per pixel point to obtain intense lipid signals can have a substantial effect on the speed of data acquisition.

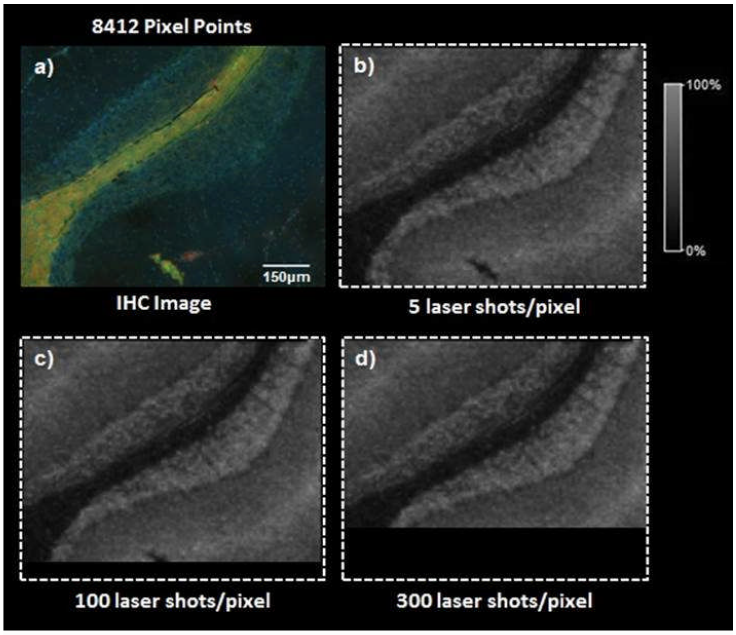


e)

| Number of laser shots per pixel | Acquisition time (min) | Acquisition speed (sec/pixel) | Percent area (8412 pixel points) imaged in 142 minutes |
|---|---|---|---|
| 5 | 142 | 1.0128 | 100% |
| 50 | 148 | 1.0554 | 96% |
| 100 | 155 | 1.1052 | 92% |
| 200 | 169 | 1.2054 | 84% |
| 300 | 183 | 1.3050 | 78% |
| 400 | 197 | 1.4051 | 72% |
| 500 | 211 | 1.5048 | 67% |

**Figure 6.** Illustration of MALDI-IMS experiment of lipids in negative ionization mode using 1,5-DAN sublimation, given with a defined a) IHC image of cerebellar region (8412 pixel points with 10µm spatial resolution) and represented by ion image of PE 38:4, m/z 766.6 b)-d). The areas indicate the approximate proportion of the cerebellar region that can be measured with indicated number of laser shots b) 5, c) 100, d) 300 per pixel point. e) comparative speed of acquisition and percent area of a cerebellar region (8412 pixel points) that can be Imaged using different number of laser shots per pixel area at 10µm spatial resolution.

Using the optimized 1,5-DAN sublimation approach, only 5 laser shots were needed for negative ion lipid imaging, reducing the required amount of time to generate a pixel spectra substantially (Figure 6b,e). Considering the number of pixel points (several tens of thousands) needed to image a whole brain tissue section at high spatial resolutions, along with the required technical- and biological replicates, this approach can substantially reduce

498 the necessary acquisition time to a more reasonable level for biological and clinical
499 applications.

500

501 **Amyloid-β Plaque Associated Neuronal Lipids Imaging Using High Spatial Resolution**
502 **MALDI-IMS with Subsequent Fluorescent Staining.** Finally, in order to further demonstrate
503 the potential and relevance of the here described method, we performed high resolution IMS
504 and subsequent fluorescent staining on brain tissue in transgenic Alzheimer's disease (AD)
505 tgSwe mice. AD is a chronic, neurodegenerative disorder which is characterized by the
506 formation of protein deposits in the brain including intercellular neurofibrillary tangles
507 consisting of hyperphosphorylated tau protein[46] and extracellular amyloid-β plaques[47].
508 Recent studies suggest that dysregulated neuronal lipid metabolism may be linked to AD
509 pathogenesis, potentially by influencing amyloidogenic processing of the transmembrane
510 amyloid precursor protein (APP) and/or the aggregation of amyloid β (Aβ).[48, 49] Therefore,
511 multimodal chemical imaging tools are needed in order to delineate Aβ plaque-associated
512 neuronal lipid species. We therefore investigated TgSwe mice that overexpress β-amyloid
513 (Aβ) due to having the human *APP* KM670/671NL mutation and develop intraneuronal Aβ
514 aggregates at six months and extracellular plaques at 12 months. We utilized the here
515 described method for rapid, high-spatial resolution (10µm), histology-compatible MALDI-IMS
516 of neuronal lipid species on a cortical region followed by subsequent fluorescent amyloid
517 staining[50] of cortical Aβ aggregates (Figure 7).

518

519

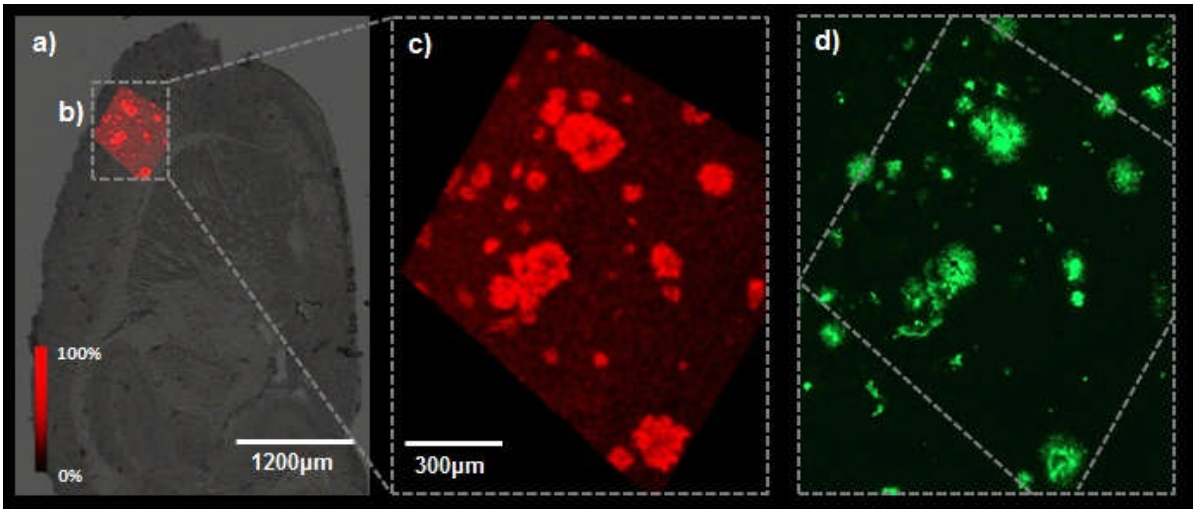


**Figure 7.** Imaging of amyloid plaque associated neuronal lipid species using high resolution MALDI-IMS with subsequent fluorescent staining. a) bright-field image of sagittal tgSwe mice brain tissue section. b) high resolution (10µm) MALDI-IMS analyzed cortical region using the method in Fig 2a IV. c,e) ion image of Ceramide (18:0, m/z 564.6) species which is correlated with d,f) high resolution fluorescent microscopy image of amyloid aggregates.

The results demonstrate a conclusive correlation of MALDI-IMS derived ion image data of e.g. ceramide species (18:0, m/z 564.6) and fluorescent microscopy images of amyloid aggregates. This in turn suggests a role of plaque-associated ceramide elevation in AD pathology as previously reported in AD patients[51] as well as in another transgenic AD models [14]. Identification of ceramide (18:0, m/z 564.6) species was based on its characteristic fragment ions[52] using MALDI-LIFT™ based MS/MS that was performed directly on the plaques in situ (Supporting Information, Figure S-7). Here, an accurate correlation of the IMS data to IHC annotated amyloid plaques is essential in order to correctly identify plaque pathology associated lipid species. This highlights further the relevance of non-impaired tissue and protein morphology as achieved with the here presented multimodal imaging methodology.

## CONCLUSIONS

In this study, we demonstrated that elaborate optimization of MALDI-IMS parameters enhanced the performance of the MALDI imaging of brain lipids. By using a comparably low-ionization energy matrix compound, 1,5-DAN, histological information after IMS analysis was

preserved along with enhanced lipid spectra quality and data acquisition speed. Subsequent immunofluorescent stainings revealed laser fluence-dependent distortion of tissue morphology, which was not detected with commonly used H&E staining. Finally, the improved methodology was successfully applied to spatially profile amyloid plaque-associated neuronal lipid species such as ceramide (Cer18:0, m/z 564.6) in a transgenic mouse model of Alzheimer's disease. The technique can be a powerful approach to probe lipid pathology of neurodegenerative diseases enhancing the corresponding information of MALDI-IMS and immunohistochemistry and/or fluorescent staining methods.

# REFERENCES


[1] van Meer, G. (2005) Cellular lipidomics, *The EMBO journal 24*, 3159-3165.
[2] Shevchenko, A., and Simons, K. (2010) Lipidomics: coming to grips with lipid diversity, *Nature reviews Molecular cell biology 11*, 593-598.
[3] Dowhan, W. (1997) Molecular basis for membrane phospholipid diversity: why are there so many lipids?, *Annual review of biochemistry 66*, 199-232.
[4] Di Paolo, G., and Kim, T.-W. (2011) Linking lipids to Alzheimer's disease: cholesterol and beyond, *Nature Reviews Neuroscience 12*, 284-296.
[5] Ruipérez, V., Darios, F., and Davletov, B. (2010) Alpha-synuclein, lipids and Parkinson's disease, *Progress in lipid research 49*, 420-428.
[6] Schmitt, F., Hussain, G., Dupuis, L., Loeffler, J. P., and Henriques, A. (2014) A plural role for lipids in motor neuron diseases: energy, signaling and structure, *Frontiers in cellular neuroscience 8*, 25.
[7] Swank, R. L., and Grimsgaard, A. (1988) Multiple sclerosis: the lipid relationship, *The American journal of clinical nutrition 48*, 1387-1393.
[8] Maxfield, F. R., and Tabas, I. (2005) Role of cholesterol and lipid organization in disease, *Nature 438*, 612-621.
[9] Caprioli, R. M., Farmer, T. B., and Gile, J. (1997) Molecular Imaging of Biological Samples: Localization of Peptides and Proteins Using MALDI-TOF MS, *Analytical Chemistry 69*, 4751-4760.
[10] McDonnell, L. A., and Heeren, R. (2007) Imaging mass spectrometry, *Mass spectrometry reviews 26*, 606-643.
[11] Chaurand, P., Cornett, D. S., Angel, P. M., and Caprioli, R. M. (2011) From whole-body sections down to cellular level, multiscale imaging of phospholipids by MALDI mass spectrometry, *Molecular & Cellular Proteomics 10*, O110. 004259.
[12] Hanrieder, J., Malmberg, P., Lindberg, O. R., Fletcher, J. S., and Ewing, A. G. (2013) Time-of-flight secondary ion mass spectrometry based molecular histology of human spinal cord tissue and motor neurons, *Analytical Chemistry 85*, 8741-8748.
[13] Hanrieder, J., Phan, N. T. N., Kurczy, M. E., and Ewing, A. G. (2013) Imaging Mass Spectrometry in Neuroscience, *ACS Chemical Neuroscience 4*, 666-679.
[14] Kaya, I., Brinet, D., Michno, W., Syvanen, S., Sehlin, D., Zetterberg, H., Blennow, K., and Hanrieder, J. (2016) Delineating Amyloid Plaque Associated Neuronal Sphingolipids In Transgenic Alzheimer's Disease Mice (tgArcSwe) Using MALDI Imaging Mass Spectrometry, *ACS Chemical Neuroscience 8*, 347-355.

[15] Hanrieder, J., Gerber, L., Persson Sandelius, Å., Brittebo, E. B., Ewing, A. G., and Karlsson, O. (2014) High resolution metabolite imaging in the hippocampus following neonatal exposure to the environmental toxin BMAA using ToF-SIMS, *ACS chemical neuroscience 5*, 568-575.
[16] Hanrieder, J., Ljungdahl, A., Fälth, M., Mammo, S. E., Bergquist, J., and Andersson, M. (2011) L-DOPA-induced dyskinesia is associated with regional increase of striatal dynorphin peptides as elucidated by imaging mass spectrometry, *Molecular & Cellular Proteomics 10*, M111. 009308.
[17] Carlred, L., Michno, W., Kaya, I., Sjövall, P., Syvänen, S., and Hanrieder, J. (2016) Probing Amyloid-β Pathology in transgenic Alzheimer's disease (tgArcSwe) mice using MALDI Imaging Mass Spectrometry, *Journal of Neurochemistry*.
[18] Yang, J., and Caprioli, R. M. (2011) Matrix sublimation/recrystallization for imaging proteins by mass spectrometry at high spatial resolution, *Analytical chemistry 83*, 5728-5734.
[19] Karas, M., and Hillenkamp, F. (1988) Laser desorption ionization of proteins with molecular masses exceeding 10,000 daltons, *Analytical chemistry 60*, 2299-2301.
[20] Thomas, A. l., Charbonneau, J. L., Fournaise, E., and Chaurand, P. (2012) Sublimation of new matrix candidates for high spatial resolution imaging mass spectrometry of lipids: enhanced information in both positive and negative polarities after 1, 5-diaminonapthalene deposition, *Analytical chemistry 84*, 2048-2054.
[21] Hankin, J. A., Barkley, R. M., and Murphy, R. C. (2007) Sublimation as a method of matrix application for mass spectrometric imaging, *Journal of the American Society for Mass Spectrometry 18*, 1646-1652.
[22] Murphy, R. C., Hankin, J. A., Barkley, R. M., and Berry, K. A. Z. (2011) MALDI imaging of lipids after matrix sublimation/deposition, *Biochimica et Biophysica Acta (BBA)-Molecular and Cell Biology of Lipids 1811*, 970-975.
[23] Deutskens, F., Yang, J., and Caprioli, R. M. (2011) High spatial resolution imaging mass spectrometry and classical histology on a single tissue section, *Journal of Mass Spectrometry 46*, 568-571.
[24] Walch, A., Rauser, S., Deininger, S.-O., and Höfler, H. (2008) MALDI imaging mass spectrometry for direct tissue analysis: a new frontier for molecular histology, *Histochemistry and cell biology 130*, 421-434.
[25] Vogel, A., and Venugopalan, V. (2003) Mechanisms of pulsed laser ablation of biological tissues, *Chemical reviews 103*, 577-644.
[26] Russo, R. E., Mao, X., Gonzalez, J. J., Zorba, V., and Yoo, J. (2013) Laser ablation in analytical chemistry, ACS Publications.
[27] Dufresne, M., Guneysu, D., Patterson, N. H., Marcinkiewicz, M. M., Regina, A., Demeule, M., and Chaurand, P. (2016) Multimodal detection of GM2 and GM3 lipid species in the brain of mucopolysaccharidosis type II mouse by serial imaging mass spectrometry and immunohistochemistry, *Analytical and Bioanalytical Chemistry*, 1-9.
[28] Dreisewerd, K. (2003) The desorption process in MALDI, *Chemical reviews 103*, 395-426.
[29] Optimizing, U. (2006) laser focus profiles for improved MALDI performance Holle, Armin; Haase, Andreas; Kayser, Markus; Hoehndorf, *Journal of Mass Spectrometry 41*, 705-716.
[30] Lord, A., Kalimo, H., Eckman, C., Zhang, X.-Q., Lannfelt, L., and Nilsson, L. N. (2006) The Arctic Alzheimer mutation facilitates early intraneuronal Aβ aggregation and senile plaque formation in transgenic mice, *Neurobiology of aging 27*, 67-77.
[31] Molin, L., Seraglia, R., Dani, F. R., Moneti, G., and Traldi, P. (2011) The double nature of 1, 5-diaminonaphthalene as matrix-assisted laser desorption/ionization matrix: some experimental evidence of the protonation and reduction mechanisms, *Rapid Communications in Mass Spectrometry 25*, 3091-3096.
[32] Soltwisch, J., Jaskolla, T. W., Hillenkamp, F., Karas, M., and Dreisewerd, K. (2012) Ion yields in UV-MALDI mass spectrometry as a function of excitation laser wavelength

and optical and physico-chemical properties of classical and halogen-substituted MALDI matrixes, *Analytical chemistry 84*, 6567-6576.
[33] Smirnov, I., Zhu, X., Taylor, T., Huang, Y., Ross, P., Papayanopoulos, I., Martin, S., and Pappin, D. (2004) Suppression of α-cyano-4-hydroxycinnamic acid matrix clusters and reduction of chemical noise in MALDI-TOF mass spectrometry, *Analytical chemistry 76*, 2958-2965.
[34] Demeure, K., Quinton, L., Gabelica, V., and De Pauw, E. (2007) Rational selection of the optimum MALDI matrix for top-down proteomics by in-source decay, *Analytical chemistry 79*, 8678-8685.
[35] Spraggins, J. M., and Caprioli, R. M. (2011) High-speed MALDI-TOF imaging mass spectrometry: rapid ion image acquisition and considerations for next generation instrumentation, *Journal of the American Society for Mass Spectrometry 22*, 1022-1031.
[36] Weickenmeier, J., de Rooij, R., Budday, S., Steinmann, P., Ovaert, T., and Kuhl, E. (2016) Brain stiffness increases with myelin content, *Acta biomaterialia 42*, 265-272.
[37] Knochenmuss, R. (2006) Ion formation mechanisms in UV-MALDI, *Analyst 131*, 966-986.
[38] Karas, M., Glückmann, M., and Schäfer, J. (2000) Ionization in matrix-assisted laser desorption/ionization: singly charged molecular ions are the lucky survivors, *Journal of Mass Spectrometry 35*, 1-12.
[39] Jaskolla, T. W., and Karas, M. (2011) Compelling evidence for lucky survivor and gas phase protonation: the unified MALDI analyte protonation mechanism, *Journal of the American Society for Mass Spectrometry 22*, 976-988.
[40] Ehring, H., Karas, M., and Hillenkamp, F. (1992) Role of photoionization and photochemistry in ionization processes of organic molecules and relevance for matrix-assisted laser desorption lonization mass spectrometry, *Organic mass spectrometry 27*, 472-480.
[41] Fischer, A. H., Jacobson, K. A., Rose, J., and Zeller, R. (2008) Hematoxylin and eosin staining of tissue and cell sections, *Cold Spring Harbor Protocols 2008*, pdb. prot4986.
[42] Chaurand, P., Schriver, K. E., and Caprioli, R. M. (2007) Instrument design and characterization for high resolution MALDI-MS imaging of tissue sections, *Journal of Mass Spectrometry 42*, 476-489.
[43] Ishizuka, I. (1997) Chemistry and functional distribution of sulfoglycolipids, *Progress in lipid research 36*, 245-319.
[44] Ogrinc Potočnik, N., Porta, T., Becker, M., Heeren, R., and Ellis, S. R. (2015) Use of advantageous, volatile matrices enabled by next-generation high-speed matrix-assisted laser desorption/ionization time-of-flight imaging employing a scanning laser beam, *Rapid Communications in Mass Spectrometry 29*, 2195-2203.
[45] Prentice, B. M., Chumbley, C. W., and Caprioli, R. M. (2016) High-speed MALDI MS/MS imaging mass spectrometry using continuous raster sampling, *Journal of Mass Spectrometry 51*, 665-665.
[46] Alonso, A. d. C., Grundke-Iqbal, I., and Iqbal, K. (1996) Alzheimer's disease hyperphosphorylated tau sequesters normal tau into tangles of filaments and disassembles microtubules, *Nature medicine 2*, 783-787.
[47] Hardy, J. A., and Higgins, G. A. (1992) Alzheimer's disease: the amyloid cascade hypothesis, *Science (New York, N.Y.) 256*, 184-185.
[48] Yadav, R. S., and Tiwari, N. K. (2014) Lipid integration in neurodegeneration: an overview of Alzheimer’s disease, *Molecular neurobiology 50*, 168-176.
[49] Hirsch-Reinshagen, V., Burgess, B. L., and Wellington, C. L. (2009) Why lipids are important for Alzheimer disease?, *Molecular and cellular biochemistry 326*, 121-129.
[50] Åslund, A., Sigurdson, C. J., Klingstedt, T., Grathwohl, S., Bolmont, T., Dickstein, D. L., Glimsdal, E., Prokop, S., Lindgren, M., and Konradsson, P. (2009) Novel pentameric

thiophene derivatives for in vitro and in vivo optical imaging of a plethora of protein aggregates in cerebral amyloidoses, *ACS chemical biology 4*, 673-684.
[51] Han, X., M Holtzman, D., W McKeel, D., Kelley, J., and Morris, J. C. (2002) Substantial sulfatide deficiency and ceramide elevation in very early Alzheimer's disease: potential role in disease pathogenesis, *Journal of neurochemistry 82*, 809-818.
[52] Woods, A. S., Colsch, B., Jackson, S. N., Post, J., Baldwin, K., Roux, A., Hoffer, B., Cox, B. M., Hoffer, M., and Rubovitch, V. (2013) Gangliosides and ceramides change in a mouse model of blast induced traumatic brain injury, *ACS chemical neuroscience 4*, 594-600.

# ASSOCIATED CONTENT

## Supporting Information

Supplementary Figure S1- S4, as noted in the text.

# AUTHOR INFORMATION

## Corresponding Author

Jörg Hanrieder, PhD

Department of Psychiatry and Neurochemistry, Sahlgrenska Academy at the University of Gothenburg, Mölndal Hospital, House V, Biskopsbogatan 27, SE-43180 Mölndal, Sweden

jh@gu.se; +46-31-343 2377

## Notes

The authors declare no competing financial interest.

# ACKNOWLEDGEMENTS

The Swedish Research Council VR (#2014-6447, JH; #2012-1593, HZ), the Royal Society of Arts and Sciences in Gothenburg (KVVS, JH), Alzheimerfonden (JH, KB), Demensfonden (JH), Hjärnfonden (KB), Jeanssons Stiftelsen (JH), Ahlén Stiftelsen (JH), Stiftelsen Gamla

Tjänarinnor (JH, KB), Stohnes Stiftelse (JH) and Stiftelsen Wilhelm och Martina Lundgrens Vetenskapsfond (JH) are acknowledged for financial support. The work was in part performed at the goIMS imaging MS infrastructure at the We thank the stuff at Centre for Cellular Imaging (CCI), Core Facilities, The Sahlgrenska Academy, University of Gothenburg, in Gothenburg, Sweden. University of Gothenburg (www.go-ims.gu.se). The authors declare no conflict of interest.

**TOC Figure:**